Single vectorlike top quark production in the tZ channel at high energy pp colliders

Bingfang Yang, Xiaoli Sima, Shiyu Wang, and Liangliang Shang*
School of Physics, Henan Normal University, Xinxiang 453007, China

(Received 9 January 2022; accepted 16 March 2022; published 12 May 2022)

In a simplified model including a singlet vectorlike top quark T with charge $|Q| = 2/3$, we investigate the single production of T decaying into tZ at the 14 TeV LHC, 27 TeV high energy LHC (HE-LHC), and 100 TeV hadron-hadron Future Circular Hadron Collider (FCC-hh). In the four flavor scheme, we make detailed detector simulations and the background analysis. We find that the excluding and discovering capability is enhanced obviously with the increase of the collision energy. The model includes only two free parameters, the coupling constant g^*, and top quark partner mass m_T. For the highest integrated luminosity designed, the excluding capability can be given as follows: (1) the LHC can exclude the correlated regions $g^* \in [0.085, 0.50]$ with $m_T \in [1000\ \text{GeV}, 1840\ \text{GeV}]$ for $\mathcal{L} = 3000\ \text{fb}^{-1}$; (2) the HE-LHC can exclude the correlated regions $g^* \in [0.035, 0.50]$ with $m_T \in [1000\ \text{GeV}, 2610\ \text{GeV}]$ for $\mathcal{L} = 15\ \text{ab}^{-1}$; (3) the FCC-hh can exclude the correlated regions $g^* \in [0.005, 0.50]$ with $m_T \in [1000\ \text{GeV}, 4270\ \text{GeV}]$ for $\mathcal{L} = 30\ \text{ab}^{-1}$. Besides, we find that the excluding and discovering regions will be reduced if the narrow width approximation limit is considered.

DOI: 10.1103/PhysRevD.105.096010

I. INTRODUCTION

The discovery of a 125 GeV Higgs boson by the ATLAS and CMS Collaborations at the Large Hadron Collider (LHC) [1] is a major step forward for explorations in the realm of particle physics. However, the gauge hierarchy problem induced by the quadratic divergence of Higgs mass still exists. To solve this problem, lots of new physics (NP) models beyond the standard model (SM) are put forward. In these models, the vector-like top quarks (VLTs) are widely introduced to cancel the largest quadratic divergence of the Higgs mass from the top quark loop [2–4] since the Higgs data at LHC excludes a fourth generation of chiral quarks. These vectorlike quarks are color-triplet spin-1/2 fermions, and the left- and right-handed components transform with the same properties under the SM electroweak symmetry group [5].

In experiment, the searches for the VLT have been performed at the LHC with $\sqrt{s} = 13$ TeV corresponding to integrated luminosity of 139 fb^{-1}. For singlet T quark, all masses below 1.8(1.6) TeV have been excluded for the universal coupling strength values above 0.5(0.41) in the decay channel $T \to tH$ or $T \to tZ$ [6]. For the $T \to Wb$ channel, the search has been performed at LHC with 13 TeV corresponding to an integrated luminosity of 36.1 fb^{-1} and set the upper limits on a singlet T quark of mass 800 GeV for the mixing angle $|\sin\theta_L| = 0.18$[7]. In phenomenology, so far, a few studies for the VLT have been performed, where the VLT is assumed to decay into either a standard mode (Wb, tZ, tH) [8–13] or some exotic channels [14–17]. Earlier, the single production of the VLT at the LHC for the five flavor scheme (5FS) has been studied in Refs. [18,19]. Since the most experiments are based on the four flavor scheme (4FS) [6,20], we will investigate the single production of the VLT decaying into tZ for the 4FS at the LHC and future pp colliders.

For a T quark with mass above 1 TeV, the daughter top quark and Z boson are highly boosted, where the top quark dominantly decays to a b quark and a W boson with the W subsequently decaying to two light quarks. These jets may lie close together since they are highly boosted and may not always be independently resolved [21]. So, the conventional reconstruction algorithms that rely on one-to-one jet-to-parton assignment may falter. In this case, the Cambridge-Aachen (C-A) algorithm [22] is often used to identify the top quark and suppress the backgrounds. So, we will adopt the C-A algorithm to reconstruct the signal and backgrounds.

The paper is organized as follows: In Sec. II, we briefly describe the simplified model including a singlet VLT and introduce the details of the event generation on the single production of T quark decaying to tZ at hadron collider; in Sec. III, we show the discovery potentiality at $\sqrt{s} = 14$ TeV [23], $\sqrt{s} = 27$ TeV [24], and $\sqrt{s} = 100$ TeV [25,26]; in Sec. IV, we give a summary.

*shangliangliang@htu.edu.cn

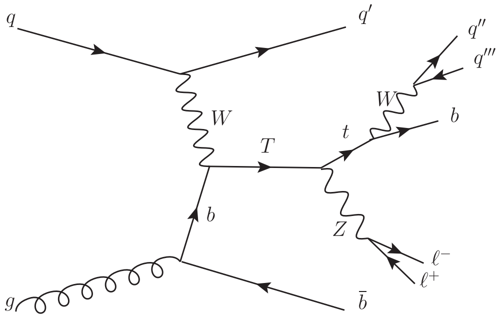

FIG. 1. The Feynman diagram of the single T quark production with subsequent decay into tZ at the pp collider.

II. EVENT GENERATION

We will study the VLT in a simplified model, which consists of an $SU(2)$ singlet VLT with the same electric charge and color as the SM top quark. In this paper, we study the vector like quarks (VLQs) that couple exclusively to third generation SM quarks and the Lagrangian of the T quark sector can be parametrized as [27]

$$\mathcal{L}_T = \frac{gg^*}{2}\left\{\frac{1}{\sqrt{2}}[\bar{T}_L W_\mu^+ \gamma^\mu b_L] + \frac{1}{2\cos\theta_W}[\bar{T}_L Z_\mu \gamma^\mu t_L] - \frac{m_T}{2m_W}[\bar{T}_R H t_L] - \frac{m_t}{2m_W}[\bar{T}_L H t_R]\right\} + \mathrm{H.c.}, \tag{1}$$

where m_T is the T quark mass, g^* parametrizes the single T production coupling associated with the SM quarks(b or t quark), g is the $SU(2)_L$ gauge coupling constant, and θ_W is the Weinberg angle. In this simplified model, the only free parameters will be the T quark mass m_T and the coupling strength g^*. Here, we take a conservative range for the coupling parameter [28]: $g^* \le 0.5$, which is consistent with the current experiment bounds. The VLT will dominantly decay to Wb, tZ and tH. For a heavy T quark, three branching ratios have a good approximation $\mathrm{Br}(T \to th) \approx \mathrm{Br}(T \to tZ) \approx \frac{1}{2}\mathrm{Br}(T \to Wb)$ as expected by Goldstone boson equivalence theorem [29].

We explore the discovery potentiality of single T production through the channel,

$$qg \to q'T(\to tZ)\bar{b} \to q't(\to bjj)Z(\to \ell^+\ell^-)\bar{b} \to 3j + 2l + 2b,$$

and show the leading-order (LO) Feynman diagram of the 4FS process in Fig. 1. We can see that the signal events contain three light jets, two b jets, and two opposite-sign and same-flavor leptons ($l = e, \mu$). According to these signal characters, we analyze the main SM backgrounds that give a pair of leptons in the final states as $Z+$jets, $t\bar{t}$, $t\bar{t}V$, VV, and $t\bar{b}Z+$jet. For the diboson events $VV(WW/WZ/ZZ)$, one of the bosons decays to hadrons, and the other decays to leptons. Besides, the potential contributions like single top ($tX, X = j, b, W$) can also be seen as backgrounds. For clarity, we summarize the signal production process and the background decay modes in Table I.

Here, it should be mentioned that we calculate the cross sections at LO for the signal using the narrow-width approximation (NWA). For the SM backgrounds, we generate the LO cross sections and then renormalize them to the next-leading-order (NLO) or the next-next-leading-order (NNLO) cross sections by multiplying by a K factor. The K factors of background cross sections mentioned in our calculation are summarized in Table II. For the cross sections at different colliders, we ignore their differences and take the same K factors for these processes.

Since the T quark is heavy, its decay products like top quark (or W, Z, H) can be boosted highly and can be

TABLE I. The processes of the signal and backgrounds.

Signal		$pp \to T(\to tZ)\bar{b}j \to t(\to bjj)Z(\to \ell^+\ell^-)\bar{b}j$			
	Backgrounds	Decay mode		Backgrounds	Decay mode
Single top	$pp \to tj$	$t \to bjj$	Diboson	$pp \to W^+W^-$	$W^+ \to \ell^+\nu_l$, $W^- \to jj$
	$pp \to tW^-$	$t \to bjj$, $W^- \to \ell^-\bar{\nu}_l$		$pp \to W^+Z$	$W^+ \to \ell^+\nu_l$, $W^- \to jj$
	$pp \to t\bar{b}$	$t \to bjj$		$pp \to ZZ$	$Z \to \ell^+\ell^-$, $Z \to jj$
Top pair	$pp \to t\bar{t}$	$t \to \ell^+\nu_l b$, $\bar{t} \to \bar{b}jj$	$Z+$jets	$pp \to Zjjj$	$Z \to \ell^+\ell^-$
	$pp \to t\bar{t}W$	$t \to \ell^+\nu_l b$, $\bar{t} \to \bar{b}jj$, $W^+ \to \ell^+\nu_l$	Other	$pp \to t\bar{b}Zj$	$t \to bjj$, $Z \to \ell^+\ell^-$
	$pp \to t\bar{t}Z$	$t \to \ell^+\nu_l b$, $\bar{t} \to \bar{b}jj$, $Z \to \ell^+\ell^-$			

TABLE II. The K factors of the QCD corrections for the background processes.

	$Z+$jets	Top pair		Single top			Diboson			Other
Processes	$Zjjj$	$t\bar{t}$	$t\bar{t}W$	$t\bar{t}Z$	tj	tW^-	$t\bar{b}$	WW	WZ	ZZ	$t\bar{b}Zj$
K factor	1.2[30]	1.8 [31]	1.2 [32,33]	1.3 [32,33]	1.4 [32,34]	1.6 [32,34]	1.9 [32,34]	1.6 [35]	1.7 [35]	1.3 [35]	1.1

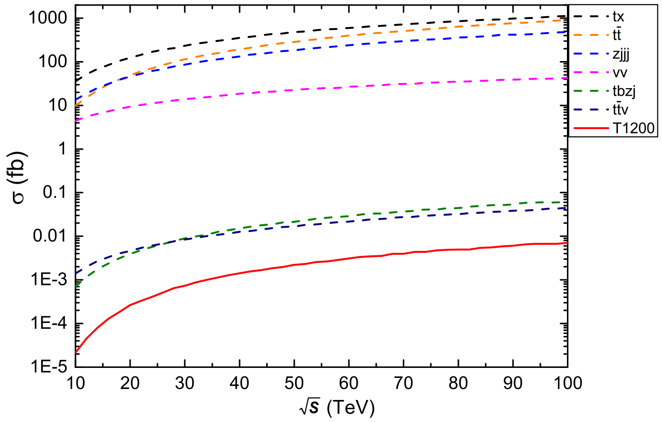

FIG. 2. Cross sections of the signal and background processes as a function of $\sqrt{s}$ for $g^* = 0.2$.

identified as a fat jet. In this kinematical regime, the conventional anti-kt reconstruction algorithm [36] is often not feasible, while the C-A algorithm is a good choice. The C-A algorithm builds the fat jet according to the following formula:

$$d_{ij} = \min(K_{T,i}^n, K_{T,j}^n)\frac{\Delta R_{ij}^2}{R^2} \tag{2}$$

$$d_{iB} = K_{T,i}^n \tag{3}$$

Here, $K_{T,i}$ is the transverse momentum of the i-th particle, ΔR_{ij} is the distance between the i and j particle, and d_{iB} is the beam distance. For the C-A algorithm, $n = 0$ and $d_{iB} = 1$.

We generate the parton-level events of the signal and backgrounds using MadGraph5-aMC@NLO [37] with the

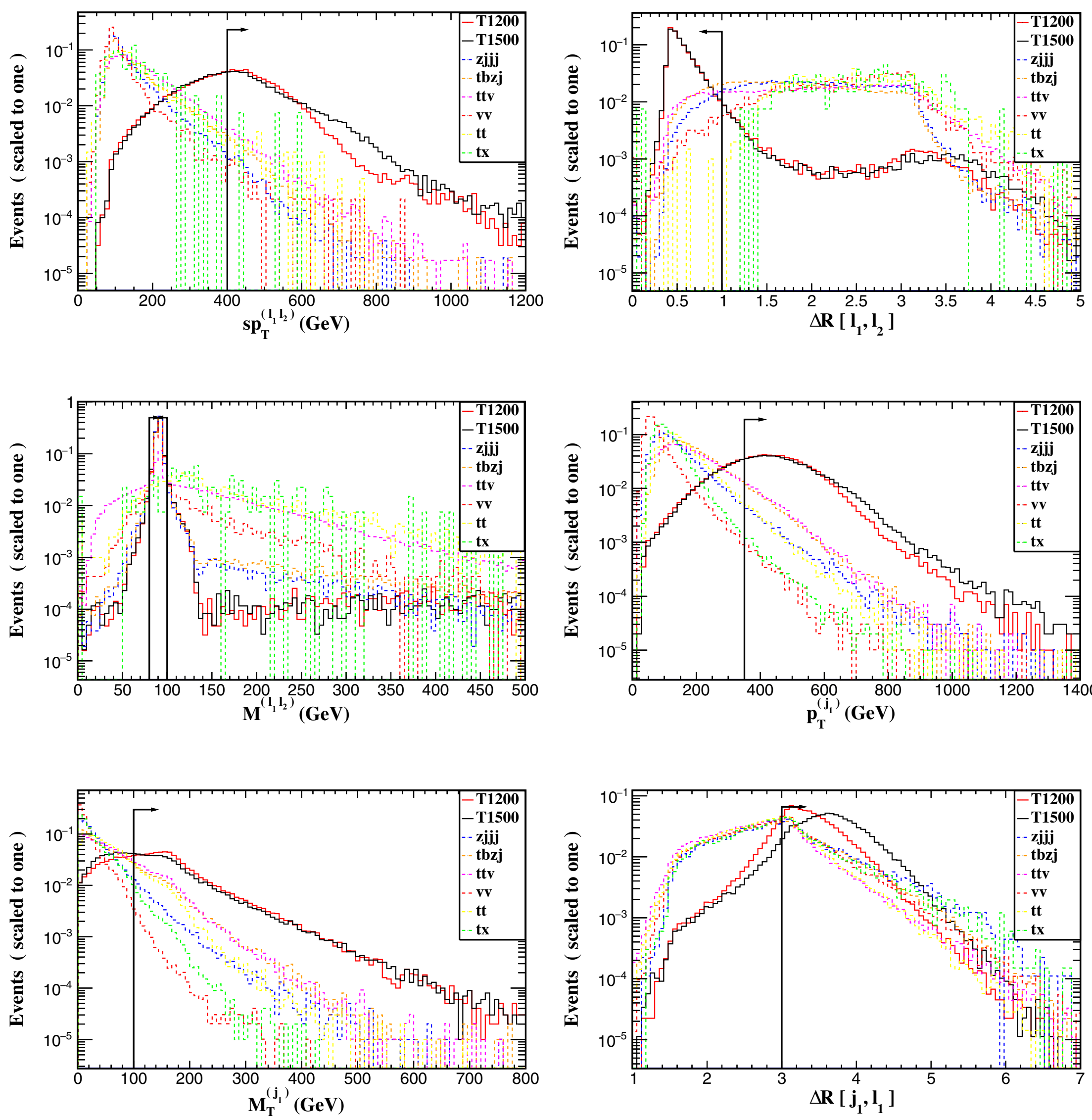

FIG. 3. Normalized distributions of $sp_T^{(\ell_1\ell_2)}$, $\Delta R[\ell_1, \ell_2]$, $M^{(\ell_1\ell_2)}$, $p_T^{(j_1)}$, $M_T^{(j_1)}$, $\Delta R[j_1, \ell_1]$ for the two signal benchmark points (T1200, T1500) and backgrounds with $g^* = 0.2$ at $\sqrt{s} = 14$ TeV.

TABLE III. Summary of the cut schemes at $\sqrt{s} = 14$ TeV.

	1000 GeV $\le m_T \le$ 2000 GeV
Trigger	$N(\ell) = 2$, $N(j) \ge 3$, $N(b) \ge 1$;
Cut-1	$sp_T^{(\ell_1 \ell_2)} > 400$ GeV, $\Delta R[\ell_1, \ell_2] < 1.0$;
Cut-2	80 GeV $< M^{(\ell_1 \ell_2)} <$ 100 GeV;
Cut-3	$p_T^{(j_1)} > 350$ GeV;
Cut-4	$M_T^{(j_1)} > 100$ GeV;
Cut-5	$\Delta R[j_1, \ell_1] > 3.0$.

parton distribution function CTEQ6_L [38]. In our calculations, the conjugate processes of signal and backgrounds have been included. We transmit these parton-level events to PYTHIA [39] for showering and hadronization, and make a fast detector simulation via DELPHES 3.14 [40]. Then, we cluster jets by FastJet [41] with the C-A algorithm, where the distance parameter $\Delta R = 1.5$. Finally, we use MadAnalysis 5 [42] to perform the event analysis. In order to connect these programs and scan the parameter space, we apply the package EasyScan_HEP [43].

For the pp colliders, we consider the following options:
(1) LHC with 3000 fb^{-1} at $\sqrt{s} = 14$ TeV,
(2) HE-LHC with 15 ab^{-1} at $\sqrt{s} = 27$ TeV,
(3) FCC-hh with 30 ab^{-1} at $\sqrt{s} = 100$ TeV.

The relevant SM input parameters are taken as follows [44]:

$$m_t = 173.0\,\mathrm{GeV},\quad m_Z = 91.1876\,\mathrm{GeV},\quad m_h = 125\,\mathrm{GeV},$$
$$\sin^2\theta_W = 0.231, \quad \alpha(m_Z) = 1/128.$$

The basic cuts at parton level for the signal and backgrounds are chosen as follows:

$$\begin{aligned} &\Delta R(x,y) > 0.4, && x,y = \ell, j, b \\ &p_T^\ell > 25\ \mathrm{GeV}, && |\eta_\ell| < 2.5 \\ &p_T^j > 25\ \mathrm{GeV}, && |\eta_j| < 5.0 \\ &p_T^b > 25\ \mathrm{GeV}, && |\eta_b| < 5.0 \end{aligned}$$

In this paper, we choose four signal benchmark points:
(i) $m_T = 1200$ GeV, $g^* = 0.2$ (labeled as T1200);
(ii) $m_T = 1500$ GeV, $g^* = 0.2$ (labeled as T1500);
(iii) $m_T = 2000$ GeV, $g^* = 0.2$ (labeled as T2000);
(iv) $m_T = 2500$ GeV, $g^* = 0.2$ (labeled as T2500).

In order to analyze the observability, we evaluate the statistical significance (SS) by using the Poisson formula as follows [45]:

$$SS = \sqrt{2L\left[(\sigma_S + \sigma_B)\ln\left(1 + \frac{\sigma_S}{\sigma_B}\right) - \sigma_S\right]}, \qquad (4)$$

where L is the integrated luminosity, and σ_S, σ_B are the signal and background cross sections after all cuts, respectively. Here, we define the exclusion limit as $SS = 2$ and the discovery significance as $SS = 5$.

III. DISCOVERY POTENTIALITY

In this section, we will study the discovery potentiality of signal at the $\sqrt{s} = 14$, 27, 100 TeV pp colliders.

A. $\sqrt{s} = 14$ TeV

In Fig. 2, we show the cross sections of the signal and background processes as a function of $\sqrt{s}$ for $g^* = 0.2$. We can see that the largest backgrounds come from tX, $t\bar{t}$, and $Zjjj$. For the tX and $t\bar{t}$, we can require the signal to include at least a pair of leptons to reduce them. For the $Zjjj$, we can reduce it through $p_T^{(j_1)}$ since we know that the signal has larger $p_T^{(j_1)}$ than this background. Besides, the b-tagging technique can be used to suppress the diboson strongly. Based on the above analysis, we choose the sum of the transverse momentum $sp_T^{(\ell_1 \ell_2)}$, the distances $\Delta R[\ell_1, \ell_2]$, $\Delta R[j_1, \ell_1]$, the invariant mass $M^{(\ell_1 \ell_2)}$, the transverse momentum $p_T^{(j_1)}$, and the transverse mass $M_T^{(j_1)}$ as selection criteria. We show these distributions in Fig. 3 and summarize the complex cuts into Table III.

TABLE IV. Cut flows of the signal benchmark points (T1200, T1500) and backgrounds for $g^* = 0.2$ at $\sqrt{s} = 14$ TeV.

	Signals (fb)	Backgrounds (fb)					
Benchmarks	T1200(T1500)	$Zjjj$	$t\bar{t}$	tX	$t\bar{t}V$	$t\bar{b}Zj$	VV
Basic cuts	0.0819 (0.0371)	26175	22357	67643	3.226	2.761	6762
Trigger	0.0287 (0.0122)	549.57	122.95	0.020	0.4286	0.7292	4.666
Cut-1	0.0149 (0.0064)	5.4682	0	0	0.0287	0.0121	0
Cut-2	0.0136 (0.0058)	4.7726	0	0	0.0025	0.0109	0
Cut-3	0.0118 (0.0051)	3.7212	0	0	0.0011	0.0069	0
Cut-4	0.0113 (0.0048)	1.4912	0	0	0.0009	0.0041	0
Cut-5	0.0071 (0.0040)	0.7456	0	0	0.0002	0.0018	0
Total efficiencies	8.67% (10.78%)	2.8×10^{-5}	0	0	6×10^{-5}	6.5×10^{-4}	0

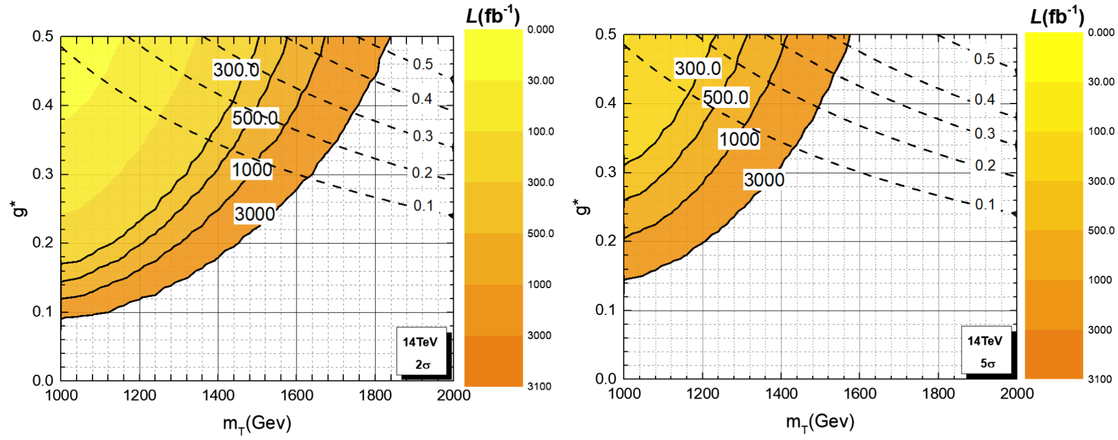

FIG. 4. The exclusion (left) and discovery (right) capabilities at $\sqrt{s} = 14$ TeV in $g^* - m_T$ plane. The solid lines denote the integrated luminosities, and the dashed lines denote the Γ_T/m_T.

We show the cut flows of the two signal benchmark points (T1200, T1500) and the backgrounds for $g^* = 0.2$ at $\sqrt{s} = 14$ TeV in Table IV. From this table, we can see that all the backgrounds can be suppressed efficiently after the selected cuts. The total cut efficiency of the signal can reach 8.67% (10.78%), while the backgrounds are reduced to $O(10^{-5})$. During the parameter scanning, we impose the uniform cuts in the parameter space.

We show the 2σ exclusion and 5σ discovery capabilities on the g^*-m_T plane at the $\sqrt{s} = 14$ TeV in Fig. 4, where the typical integrated luminosities and the width-to-mass ratios Γ_T/m_T are also displayed. We can see that the T quark can be excluded in the correlated regions of $g^* \in [0.172, 0.50]$ and $m_T \in [1000\ \text{GeV}, 1510\ \text{GeV}]$ with the integrated luminosity of 300 fb^{-1}. If the integrated luminosity of 3000 fb^{-1} can be reached, that is, at high luminosity LHC (HL-LHC), the excluded regions can be expanded to $g^* \in [0.085, 0.50]$ and $m_T \in [1000\ \text{GeV}, 1840\ \text{GeV}]$. At the HL-LHC, the discovered correlated regions can be expanded to $g^* \in [0.15, 0.50]$ and $m_T \in [1000\ \text{GeV}, 1570\ \text{GeV}]$. For clarity, we summarize these results in Table V.

Since the widths of VLT may be large and not negligible, we also need to consider the NWA limit. If the search at the HL-LHC is sensitive to the width-to-mass ratios ranging from narrow up to 30%, the excluded (discovered) parameter space mentioned above will be reduced to $g^* \in [0.085, 0.39]$ ([0.15,0.45]) and $m_T \in$ [1000 GeV, 1720 GeV] ([1000 GeV, 1520 GeV]).

B. $\sqrt{s} = 27$ TeV

We take the distributions $sp_T^{(\ell_1\ell_2)}$, $\Delta R[\ell_1, \ell_2]$, $M^{(\ell_1\ell_2)}$, $\Delta R[j_1, \ell_1]$, $sp_T^{(j_1j_2j_3)}$, the missing transverse energy $\not{E}_T$ as selection criteria, and show these normalized distributions of the signal and backgrounds for $g^* = 0.2$ at $\sqrt{s} =$ 27 TeV in Fig. 5. According to the behavioral characteristics of these distributions, we impose the complex cuts shown in the Table VI to get a high significance.

We show the cut flows of the two signal benchmark points (T1500, T2000) and the backgrounds for $g^* = 0.2$ at $\sqrt{s} = 27$ TeV in Table VII. We can see that the total cut efficiency of signal can reach more than 10,000 times that of the backgrounds. We shows the exclusion and discovery capabilities on the g^*-m_T plane at $\sqrt{s} = 27$ TeV in Fig. 6 and summarize the typical results in Table VIII. Compared to the HL-LHC, we can see that the excluded (discovered) regions of the T quark can be expanded to $g^* \in [0.063, 0.50]$([0.10, 0.50]) and $m_T \in [1000\ \text{GeV}, 2330\ \text{GeV}]$ ([1000 GeV, 2000 GeV]) with the integrated luminosity of 3000 fb^{-1}. If the high integrated luminosity of 15 ab^{-1}

TABLE V. The excluding and discovering capabilities on T at LHC.

LHC ($\sqrt{s} = 14$ TeV) $m_T \in [1000, 2000]$ GeV		
	2σ	5σ
g^* ($\mathcal{L} = 300$ fb^{-1})	[0.172,0.50]	[0.310,0.50]
g^* ($\mathcal{L} = 500$ fb^{-1})	[0.150,0.50]	[0.260,0.50]
g^* ($\mathcal{L} = 1000$ fb^{-1})	[0.110,0.50]	[0.200,0.50]
g^* ($\mathcal{L} = 3000$ fb^{-1})	[0.085,0.50]	[0.150,0.50]

TABLE VI. Summary of the cut schemes at $\sqrt{s} = 27$ TeV.

	1000 GeV $\le m_T \le$ 3500 GeV
Trigger	$N(\ell) = 2$, $N(j) \ge 3$, $N(b) \ge 1$;
Cut-1	$sp_T^{(\ell_1\ell_2)} > 400$ GeV, $\Delta R[\ell_1, \ell_2] < 1.0$;
Cut-2	80 GeV $< M^{(\ell_1\ell_2)} <$ 100 GeV;
Cut-3	$\Delta R[j_1, \ell_1] > 3.1$;
Cut-4	$sp_T^{(j_1j_2j_3)} < 650$ GeV;
Cut-5	$\not{E}_T > 40$ GeV.

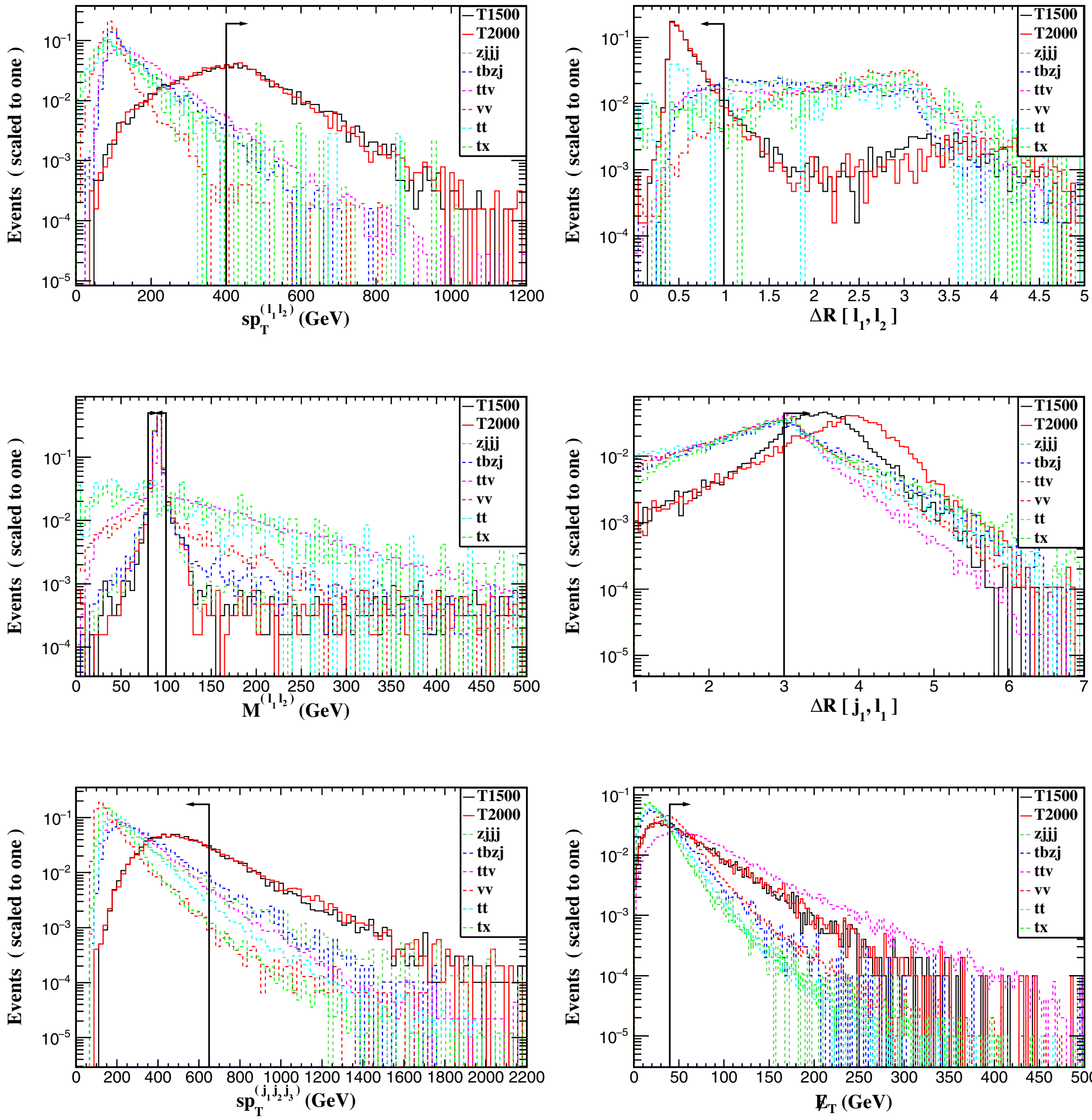

FIG. 5. Normalized distributions of $sp_T^{(\ell_1\ell_2)}$, $\Delta R[\ell_1,\ell_2]$, $M^{(\ell_1\ell_2)}$, $\Delta R[j_1,\ell_1]$, $sp_T^{(j_1j_2j_3)}$, $\not{E}_T$ for the two signal benchmark points (T1500,T2000) and backgrounds with $g^* = 0.2$ at $\sqrt{s} = 27$ TeV.

TABLE VII. Cut flows of two signal benchmark points (T1500, T2000) and backgrounds for $g^* = 0.2$ at $\sqrt{s} = 27$ TeV.

	Signals (fb)	Backgrounds (fb)					
Benchmarks	T1500(2000)	$Zjjj$	$t\bar{t}$	tX	$t\bar{t}V$	$t\bar{b}Zj$	VV
Basic cuts	0.1605 (0.0704)	81552	242736	197906	9.95	11.843	12267
Trigger	0.0833 (0.0362)	3849.3	495.18	235.0	3.8277	5.6241	3.4921
Cut-1	0.0422 (0.0183)	166.63	0	0	0.0316	0.1232	0
Cut-2	0.0394 (0.0169)	149.97	0	0	0.0270	0.1148	0
Cut-3	0.0264 (0.0138)	61.098	0	0	0.0085	0.0450	0
Cut-4	0.0204 (0.0101)	27.769	0	0	0.0075	0.0320	0
Cut-5	0.0127 (0.0063)	5.5538	0	0	0.0063	0.0165	0
Total efficiencies	7.91% (8.95%)	6.8×10^{-5}	0	0	6.4×10^{-4}	1.4×10^{-3}	0

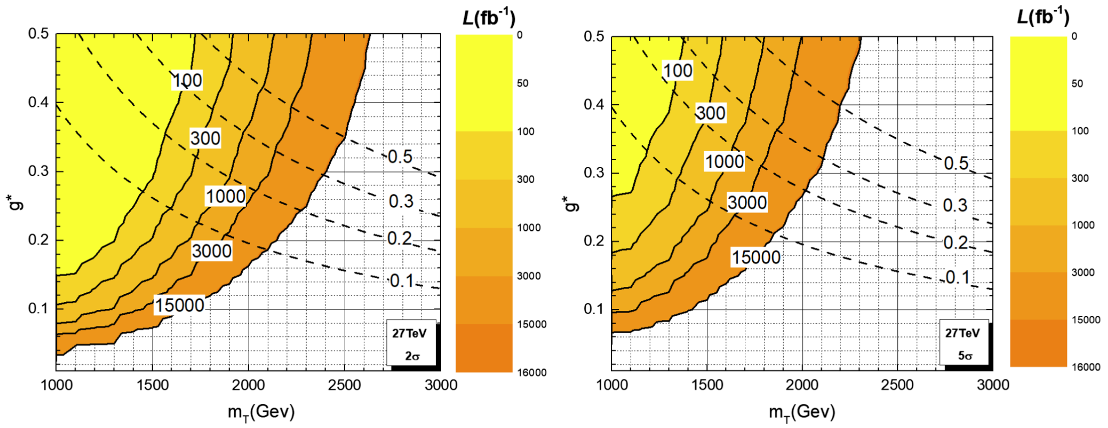

FIG. 6. Same as Fig. 4, but for $\sqrt{s} = 27$ TeV.

can be reached, the larger regions $g^* \in [0.035, 0.50] \times ([0.04, 0.50])$ and $m_T \in [1000\ \mathrm{GeV}, 2630\ \mathrm{GeV}]([1000\ \mathrm{GeV}, 2300\ \mathrm{GeV}])$ can be excluded (discovered). If we consider $\Gamma_T/m_T < 30\%$, the excluded (discovered) regions will be reduced to $g^* \in [0.035, 0.28]$ ($[0.065, 0.32]$) and $m_T \in [1000\ \mathrm{GeV}, 2400\ \mathrm{GeV}]([1000\ \mathrm{GeV}, 2100\ \mathrm{GeV}])$.

TABLE VIII. The excluding and discovering capabilities on T at HE-LHC.

LHC ($\sqrt{s} = 27$ TeV)$m_T \in [1000, 3500]$ GeV		
	2σ	5σ
g^* ($\mathcal{L} = 300$ fb^{-1})	[0.100,0.50]	[0.175,0.50]
g^* ($\mathcal{L} = 1000$ fb^{-1})	[0.075,0.50]	[0.125,0.50]
g^* ($\mathcal{L} = 3000$ fb^{-1})	[0.065,0.50]	[0.100,0.50]
g^* ($\mathcal{L} = 15$ ab^{-1})	[0.035,0.50]	[0.040,0.50]

TABLE IX. Summary of the cut schemes at $\sqrt{s} = 100$ TeV.

	1000 GeV $\le m_T \le$ 5000 GeV
Trigger	$N(\ell) = 2$, $N(j) \ge 3$, $N(b) \ge 1$;
Cut-1	$sp_T^{(\ell_1\ell_2)} > 400$ GeV, $\Delta R[\ell_1, \ell_2] < 1.0$;
Cut-2	75 GeV $< M^{(\ell_1\ell_2)} <$ 105 GeV;
Cut-3	$\Delta R[j_1, \ell_1] > 3.1$;
Cut-4	$sp_T^{(j_1j_2j_3)} < 850$ GeV.

C. $\sqrt{s} = 100$ TeV

We take the distributions $sp_T^{(\ell_1\ell_2)}$, $\Delta R[\ell_1, \ell_2]$, $M^{(\ell_1\ell_2)}$, $\Delta R[j_1, \ell_1]$, and $sp_T^{(j_1j_2j_3)}$ as selection criterias. Since the behavior of these kinematic distributions at FCC-hh are similar to the HE-LHC, we do not show them here again. According to the behaviors of these distributions, we impose some complex cuts shown in Table IX to enhance the significance and show the cut flows of the signal and backgrounds in Table X. We can see that the total cut efficiency of the signal can reach 7.40% or 8.15% for the benchmark points, while the total cut efficiencies of the backgrounds are reduced to $\mathcal{O}(10^{-4})$ or even smaller.

We show the exclusion and discovery capabilities in $g^* - m_T$ plane at $\sqrt{s} = 100$ TeV in Fig. 7 and summarize the typical results in Table XI. For the integrated luminosity of 3000 fb^{-1} (15 ab^{-1}), we can see that the T quark can be excluded in the regions of $g^* \in [0.015, 0.50]([0.01, 0.50])$ and $m_T \in [1000\ \mathrm{GeV}, 3680\ \mathrm{GeV}]([1000\ \mathrm{GeV}, 4100\ \mathrm{GeV}])$. If the high integrated luminosity of 30 ab^{-1} can be reached, the excluded regions can be be expanded to $g^* \in [0.005, 0.50]$ and $m_T \in [1000\ \mathrm{GeV}, 4270\ \mathrm{GeV}]$. Compared to the

TABLE X. Cut flows of two signal benchmark points (T2000, T2500) and backgrounds for $g^* = 0.2$ at $\sqrt{s} = 100$ TeV.

	Signals (fb)	Backgrounds (fb)					
Benchmarks	T1500(2500)	$Zjjj$	$t\bar{t}$	tX	$t\bar{t}V$	$t\bar{b}Zj$	VV
Basic cuts	2.388 (0.1748)	569103	900436	1109324	28.547	26.93	41995
Trigger	0.6789 (0.0378)	28625	67532	12340	5.0613	5.488	152.57
Cut-1	0.3506 (0.0210)	478.05	0	0	0.0742	0.0485	0
Cut-2	0.3362 (0.0201)	478.05	0	0	0.0685	0.0458	0
Cut-3	0.2075 (0.0166)	95.610	0	0	0.0171	0.0081	0
Cut-4	0.1767 (0.0142)	38.244	0	0	0.0171	0.0054	0
Total efficiencies	7.40% (8.15%)	6.7×10^{-5}	0	0	6×10^{-4}	2×10^{-4}	0

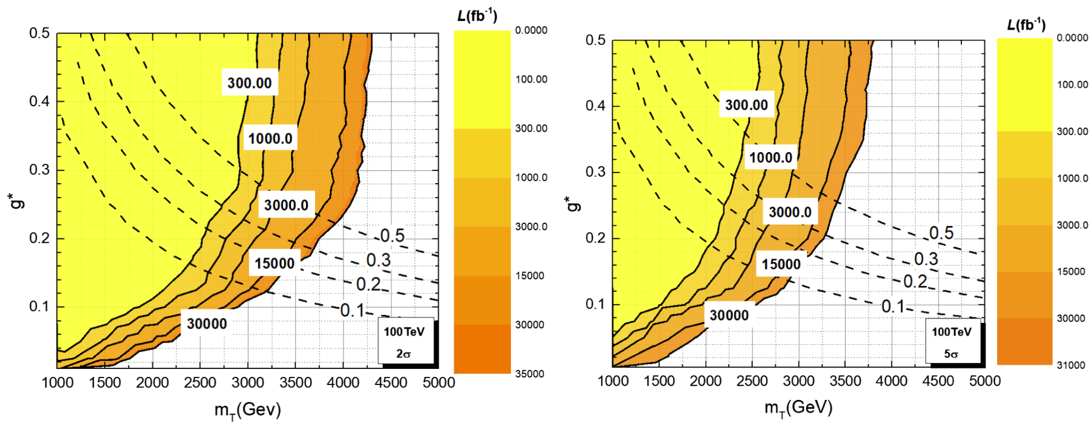

FIG. 7. Same as Fig. 4, but for $\sqrt{s} = 100$ TeV.

TABLE XI. The excluding and discovering capabilities on T at FCC-hh.

FCC-hh ($\sqrt{s} = 100$ TeV) $m_T \in [1000, 5000]$ GeV		
	2σ	5σ
g^* ($\mathcal{L} = 300$ fb^{-1})	[0.020,0.50]	[0.025,0.50]
g^* ($\mathcal{L} = 3000$ fb^{-1})	[0.015,0.50]	[0.020,0.50]
g^* ($\mathcal{L} = 15$ ab^{-1})	[0.010,0.50]	[0.015,0.50]
g^* ($\mathcal{L} = 30$ ab^{-1})	[0.005,0.50]	[0.010,0.50]

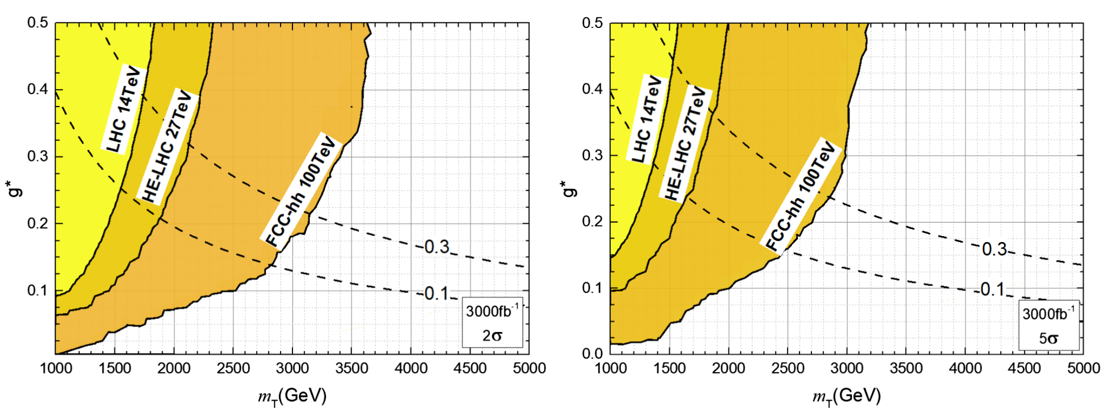

FIG. 8. Comparison of the exclusion (left) and discovery (right) capability in $g*$-m_T plane at $\sqrt{s} = 14$, 27, 100 TeV with the integrated luminosity of 3000 fb^{-1}. The dashed lines denote the Γ_T/m_T.

TABLE XII. Comparison of the excluding and discovering capabilities on T at different colliders and flavor schemes.

	Excluding capability (2σ)		Discovering capability (5σ)	
Colliders	LHC ($\sqrt{s} = 14$ TeV)	FCC-hh ($\sqrt{s} = 100$ TeV)	LHC ($\sqrt{s} = 14$ TeV)	FCC-hh ($\sqrt{s} = 100$ TeV)
Luminosity	$\mathcal{L} = 1000\ \mathrm{fb}^{-1}$	$\mathcal{L} = 30\ \mathrm{ab}^{-1}$	$\mathcal{L} = 1000\ \mathrm{fb}^{-1}$	$\mathcal{L} = 30\ \mathrm{ab}^{-1}$
m_T(GeV)	[1000,1500]	[1300,3000]	[1000,1400]	[1300,3000]
4FS(g^*)	[0.090,0.31]	[0.005,0.11]	[0.142,0.48]	[0.01,0.17]
5FS(g^*)	[0.105,0.34]	[0.040,0.26]	[0.195,0.50]	[0.060,0.45]

HL-LHC and HE-LHC, the discovery capability of the T quark at the FCC-hh has also been improved greatly. If we consider the NWA limit $\Gamma_T/m_T < 30\%$, the excluded (discovered) regions will be reduced to $g^* \in [0.005, 0.18]$ ($[0.01, 0.21]$) and $m_T \in [1000\ \mathrm{GeV}, 3670\ \mathrm{GeV}]$ ($[1000\ \mathrm{GeV}, 3270\ \mathrm{GeV}]$) with the integrated luminosity of 30 ab^{-1}.

IV. SUMMARY

In this paper, we studied the single production of T quark in the tZ channel at the LHC, HE-LHC, and FCC-hh in 4FS. We perform a detailed detector simulation of the signal and backgrounds and obtained the excluding and discovering capabilities on the T quark at different colliders. For comparison, we show the exclusion and discovery capabilities on g^*-m_T plane with the integrated luminosity of 3000 fb^{-1} at $\sqrt{s} = 14$ TeV, 27 TeV, 100 TeV in Fig. 8. We can see that the excluding and discovering capabilities are enhanced obviously with the increase of the collision energy. For the typical coupling $g^* = 0.1(0.2)$, the LHC 14 TeV can exclude the m_T up to 1160 GeV (1430 GeV), the HE-LHC 27 TeV can exclude the m_T up to 1450 GeV (1850 GeV), and the FCC-hh 100 TeV can exclude the m_T up to 2500 GeV (3140 GeV).

Besides, we compare the excluding and discovering capabilities on the T quark at different colliders for the 4FS and 5FS in Table XII. We can see that the excluding and discovering capabilities for the 4FS in our work are stronger than that for the 5FS. We expect our analysis can provide a complementary candidate to pursue the search and mass measurement of a possible singlet VLT at the future hadron colliders.

ACKNOWLEDGMENTS

This work is supported by the National Natural Science Foundation of China (NNSFC) under Grant No. 11705048, the National Research Project Cultivation Foundation of Henan Normal University under Grants No. 2020PL16, No. 2021PL10, the Startup Foundation for Doctors of Henan Normal University under Grant No. qd18115, and also powered by the High Performance Computing Center of Henan Normal University.

[1] G. Aad *et al.* (ATLAS Collaboration), Phys. Lett. B **716**, 1 (2012).
[2] N. Arkani-Hamed, A. G. Cohen, E. Katz, and A. E. Nelson, J. High Energy Phys. 07 (2002) 034.
[3] K. Agashe, G. Perez, and A. Soni, Phys. Rev. D **75**, 015002 (2007).
[4] M. Low, A. Tesi, and L. T. Wang, Phys. Rev. D **91**, 095012 (2015).
[5] J. A. Aguilar-Saavedra, R. Benbrik, S. Heinemeyer, and M. Pérez-Victoria, Phys. Rev. D **88**, 094010 (2013).
[6] ATLAS Collaboration, Report No. ATLAS-CONF-2021-040.
[7] M. Aaboud *et al.* (ATLAS Collaboration), J. High Energy Phys. 05 (2019) 164.
[8] O. Matsedonskyi, G. Panico, and A. Wulzer, J. High Energy Phys. 12 (2014) 097.
[9] T. Andeen, C. Bernard, K. Black, T. Childres, L. Dell'Asta, and N. Vignaroli, arXiv:1309.1888.
[10] N. Vignaroli, J. High Energy Phys. 07 (2012) 158.
[11] N. Vignaroli, Phys. Rev. D **86**, 075017 (2012).
[12] A. De Simone, O. Matsedonskyi, R. Rattazzi, and A. Wulzer, J. High Energy Phys. 04 (2013) 004.
[13] A. Buckley, J. M. Butterworth, L. Corpe, D. Huang, and P. Sun, SciPost Phys. **9**, 069 (2020).
[14] A. Senol, A. T. Tasci, and F. Ustabas, Nucl. Phys. **B851**, 289 (2011).
[15] J. Alwall, J. L. Feng, J. Kumar, and S. Su, Phys. Rev. D **81**, 114027 (2010).
[16] N. Liu, L. Wu, B. Yang, and M. Zhang, Phys. Lett. B **753**, 664 (2016).
[17] A. M. Sirunyan *et al.* (CMS Collaboration), J. High Energy Phys. 04 (2017) 136.
[18] Y. B. Liu and Y. Q. Li, Eur. Phys. J. C **77**, 654 (2017).
[19] X. Y. Tian, L. F. Du, and Y. B. Liu, Nucl. Phys. **B965**, 115358 (2021).
[20] A. M. Sirunyan *et al.* (CMS Collaboration), Phys. Lett. B **781**, 574 (2018).

[21] D. E. Kaplan, K. Rehermann, M. D. Schwartz, and B. Tweedie, Phys. Rev. Lett. **101**, 142001 (2008).
[22] CMS Collaboration, Report No. CMS-PAS-JME-09-001.
[23] I. Zurbano Fernandez, M. Zobov, A. Zlobin, F. Zimmermann, M. Zerlauth, C. Zanoni, C. Zannini, O. Zagorodnova, I. Zacharov, and M. Yu *et al.*, CERN Yellow Rep. Monogr. **10** (2020), 10.23731/CYRM-2020-0010.
[24] X. Cid Vidal, M. D. Onofrio, P. J. Fox, R. Torre, K. A. Ulmer, A. Aboubrahim, A. Albert, J. Alimena, B. C. Allanach, and C. Alpigiani *et al.*, CERN Yellow Rep. Monogr. **7**, 585 (2019).
[25] Future circular collider study, https://fcc.web.cern.ch/Pages/default.aspx.
[26] M. Bicer *et al.* (TLEP Design Study Working Group), J. High Energy Phys. 01 (2014) 164.
[27] M. Buchkremer, G. Cacciapaglia, A. Deandrea, and L. Panizzi, Nucl. Phys. **B876**, 376 (2013).
[28] ATLAS Collaboration, Report No. ATLAS-CONF-2016-072.
[29] B. W. Lee, C. Quigg, and H. B. Thacker, Phys. Rev. D **16**, 1519 (1977).
[30] J. Alwall, R. Frederix, S. Frixione, V. Hirschi, F. Maltoni, O. Mattelaer, H. S. Shao, T. Stelzer, P. Torrielli, and M. Zaro, J. High Energy Phys. 07 (2014) 079.
[31] M. Czakon and A. Mitov, J. High Energy Phys. 12 (2012) 054.
[32] N. Kidonakis, arXiv:1808.02934.
[33] J. M. Campbell and R. K. Ellis, J. High Energy Phys. 07 (2012) 052.
[34] E. Boos and L. Dudko, Int. J. Mod. Phys. A **27**, 1230026 (2012).
[35] J. M. Campbell and R. K. Ellis, Phys. Rev. D **60**, 113006 (1999).
[36] M. Cacciari and G. P. Salam, Phys. Lett. B **641**, 57 (2006).
[37] J. Alwall, R. Frederix, and S. Frixione, V. Hirschi, F. Maltoni, O. Mattelaer, H.-S. Shao, T. Stelzer, P. Torrielli, and M. Zaro, J. High Energy Phys. 07 (2014) 079.
[38] J. Pumplin, A. Belyaev, J. Huston, D. Stump, and W. K. Tung, J. High Energy Phys. 02 (2006) 032.
[39] T. Sjostrand, S. Mrenna, and P. Z. Skands, J. High Energy Phys. 05 (2006) 026.
[40] J. D. Favereau, C. Delaere, and P. Demin, A. Giammanco, V. Lemaître, A. Mertens, and M. Selvaggi (DELPHES 3 Collaboration), J. High Energy Phys. 02 (2014) 057.
[41] M. Cacciari, G. P. Salam, and G. Soyez, Eur. Phys. J. C **72**, 1896 (2012).
[42] E. Conte, B. Fuks, and G. Serret, Comput. Phys. Commun. **184**, 222 (2013).
[43] L. Shang and Y. Zhang, EasyScan HEP, https://easyscanhep.hepforge.org.
[44] M. Tanabashi *et al.* (Particle Data Group), Phys. Rev. D **98**, 030001 (2018).
[45] G. Cowan, K. Cranmer, E. Gross, and O. Vitells, Eur. Phys. J. C **71**, 1554 (2011).